ANALYTICAL PERFORMANCE EVALUATION FOR HOSVD-BASED PARAMETER ESTIMATION SCHEMES

Florian Roemer, Hanna Becker, Martin Haardt, and Martin Weis

Ilmenau University of Technology, Communications Research Laboratory
P.O. Box 100565, D-98684 Ilmenau, Germany, http://tu-ilmenau.de/crl
{florian.roemer,hanna.becker,martin.haardt,martin.weis}@tu-ilmenau.de

***Abstract* — Subspace-based high-resolution parameter estimation schemes are used in a variety of signal processing applications including radar, sonar, communications, medical imaging, and the estimation of the parameters of the dominant multipath components from MIMO channel sounder measurements. It is of great theoretical and practical interest to predict the performance of these schemes analytically. Since they rely on the estimate of the signal subspace obtained via a singular value decomposition (SVD), significant contributions to the perturbation analysis of the SVD have been made in the last decades.**

Recently, we have shown that in multidimensional harmonic retrieval problems, the measurement matrix can be replaced by a measurement tensor which allows to exploit the natural multidimensional structure of the data. Replacing the SVD by a multidimensional extension known as Higher-Order SVD (HOSVD) gives rise to the class of HOSVD-based parameter estimation schemes such as R-D standard Tensor-ESPRIT and R-D Unitary Tensor-ESPRIT ($R \geq 2$).

To study the performance of these tensor-based methods, an extension of the performance analysis for the matrix signal subspace (computed from the SVD) to the tensor signal subspace (computed from the HOSVD) is required. In this paper we demonstrate how an arbitrary first order perturbation analysis for the SVD can be transformed into the corresponding prediction for the HOSVD. As an example, we demonstrate the performance assessment for 2-D standard Tensor-ESPRIT and compare analytical results with simulation results. The results can be extended to the evaluation of any HOSVD-based parameter estimation scheme.

Index Terms— Perturbation analysis, HOSVD, ESPRIT

1. INTRODUCTION

High resolution parameter estimation from R-dimensional (R-D) signals is a task required for a variety of applications, such as estimating the multi-dimensional parameters of the dominant multipath components from MIMO channel sounder measurements [4], which may be used for geometry-based channel modeling. In this example, the propagation scenario is modeled as a superposition of a finite number of dominant planar wavefronts. Each of these may be characterized by an azimuth and an elevation angle at the transmitter (direction of departure), an azimuth and an elevation angle at the receiver (direction of arrival), a propagation delay, and a Doppler shift, which gives rise to a $R = 6$ dimensional harmonic retrieval problem [4]. Other applications include radar, wireless communications [7], sonar, seismology, and medical imaging. In [3] we have shown that instead of stacking the multidimensional measurements along the rows of a measurement matrix, a measurement tensor should be used since this preserves the multidimensional structure of the data. Based on the measurement tensor, this structure can be exploited to improve the estimation accuracy of the signal subspace by replacing the SVD by the Higher-Order SVD (HOSVD) [1]. This gives rise to a family of HOSVD-based subspace estimation schemes, e.g., R-D standard Tensor-ESPRIT and R-D Unitary Tensor-ESPRIT.

So far, the performance of these tensor-based schemes has been evaluated only via simulations [3, 8]. It is desirable to find an analytical characterization of the achievable estimation accuracy similar to the perturbation analysis based approaches known from matrix-based algorithms. We therefore have to extend the perturbation analysis for the matrix signal subspace computed via the SVD to the tensor signal subspace computed via the HOSVD.

Perturbation analysis for the SVD has a long standing history in the signal processing literature. For instance, [2] provides the statistics of eigenvectors of the sample covariance matrices. A first order perturbation of the invariance subspace is given in [5], the extension to a second order analysis is provided in [10], [11]. Both first and second order analysis have in common that the contribution of the noise subspace to the error of the signal subspace is on the first order of the perturbation of the data matrix. Moreover, the contribution of the signal subspace to the error of the signal subspace is on the second order of the perturbation of the data matrix so that this contribution can be ignored when first-order perturbation is studied. In [6] it is shown that there is also an impact of the signal subspace to the error of the signal subspace which is on the first order of the perturbation of the data matrix under more relaxed assumptions. Since we provide a general framework how to extend first-order matrix-based performance assessment to the tensor-case one can choose to use [5] or [6]. Note that conditions on the eigenvalue spread under which [5] is sufficient are provided in [6]. Moreover, even though [6] may provide a more accurate estimate of the individual singular vectors, the subspace is unchanged and hence there is no impact on the performance of subspace-based algorithms such as ESPRIT or MUSIC.

As an example, we use the analytical performance assessment for ESPRIT from [5] together with the new results on the tensor subspace to predict the performance of 2-D standard Tensor-ESPRIT. To demonstrate the validity of our results, we compare the analytical estimation errors with simulation results at the end of this paper.

2. NOTATION

To distinguish between scalars, vectors, matrices, and tensors, the following notation is used throughout the paper: Scalars are denoted as italic letters (a, b, A, B), vectors as lower-case bold-faced

The authors gratefully acknowledge the partial support of the German Research Foundation (Deutsche Forschungsgemeinschaft, DFG) under contract no. HA 2239/2-1.

letters ($\boldsymbol{a}, \boldsymbol{b}$), matrices are represented by upper-case bold-faced letters ($\boldsymbol{A}, \boldsymbol{B}$), and tensors are written as bold-faced calligraphic letters ($\boldsymbol{\mathcal{A}}, \boldsymbol{\mathcal{B}}$).

The superscripts ${}^{\mathrm{T}}, {}^{\mathrm{H}}, {}^{-1}$ represent matrix transposition, Hermitian transposition, and matrix inversion, respectively. Moreover, * denotes the complex conjugate operator. The Kronecker product, the Khatri-Rao (columnwise Kronecker) product, and the Schur (elementwise) product between two matrices $\boldsymbol{A}$ and $\boldsymbol{B}$ are represented by $\boldsymbol{A} \otimes \boldsymbol{B}$, $\boldsymbol{A} \diamond \boldsymbol{B}$, and $\boldsymbol{A} \odot \boldsymbol{B}$, respectively.

An R-dimensional tensor $\boldsymbol{\mathcal{A}} \in \mathbb{C}^{M_1 \times M_2 \ldots \times M_R}$ is an R-way array of size M_r along mode r. The r-mode vectors of $\boldsymbol{\mathcal{A}}$ are obtained by varying the r-th index and keeping all other indices fixed. Collecting all r-mode vectors into a matrix we obtain the r-mode unfolding of $\boldsymbol{\mathcal{A}}$ which is represented by $[\boldsymbol{\mathcal{A}}]_{(r)} \in \mathbb{C}^{M_r \times M_{r+1} \cdot \ldots \cdot M_R \cdot M_1 \cdot \ldots \cdot M_{r-1}}$. The ordering of the columns in $[\boldsymbol{\mathcal{A}}]_{(r)}$ is chosen in accordance with [1]. The r-rank of $\boldsymbol{\mathcal{A}}$ is defined as the rank of $[\boldsymbol{\mathcal{A}}]_{(r)}$. Note that in general, all the r-ranks of a tensor $\boldsymbol{\mathcal{A}}$ can be different.

The r-mode product between a tensor $\boldsymbol{\mathcal{A}} \in \mathbb{C}^{M_1 \times M_2 \ldots \times M_R}$ and a matrix $\boldsymbol{U}_r \in \mathbb{C}^{P_r \times M_r}$ is symbolized by $\boldsymbol{\mathcal{B}} = \boldsymbol{\mathcal{A}} \times_r \boldsymbol{U}_r$. It is computed by multiplying all r-mode vectors from the left-hand side by the matrix $\boldsymbol{U}_r$, i.e., $[\boldsymbol{\mathcal{B}}]_{(r)} = \boldsymbol{U}_r \cdot [\boldsymbol{\mathcal{A}}]_{(r)}$.

The Higher-Order SVD (HOSVD) of a tensor $\boldsymbol{\mathcal{A}} \in \mathbb{C}^{M_1 \times M_2 \ldots \times M_R}$ is given by

$$\boldsymbol{\mathcal{A}} = \boldsymbol{\mathcal{S}} \times_1 \boldsymbol{U}_1 \times_2 \boldsymbol{U}_2 \ldots \times_R \boldsymbol{U}_R,$$

where $\boldsymbol{\mathcal{S}} \in \mathbb{C}^{M_1 \times M_2 \ldots \times M_R}$ is the core tensor, which satisfies the all-orthogonality conditions [1] and $\boldsymbol{U}_r \in \mathbb{C}^{M_r \times M_r}$ are the unitary matrices of r-mode singular vectors for $r = 1, 2, \ldots, R$.

The tensor $\boldsymbol{\mathcal{I}}_{R,d}$ is the R-dimensional identity tensor of size $d \times d \times \ldots \times d$, which is equal to one if all indices are equal and zero otherwise.

3. DATA MODEL

We assume that we observe a linear mixture of d sources observed at $N \geq d$ subsequent time instants via an R-D array of M sensor elements. By stacking the R dimensions along the rows of the measurement matrix $\boldsymbol{X} \in \mathbb{C}^{M \times N}$ we obtain the following model

$$\boldsymbol{X} = \boldsymbol{A} \cdot \boldsymbol{S} + \boldsymbol{N}, \tag{1}$$

where $\boldsymbol{S} \in \mathbb{C}^{d \times N}$ contains the source symbols and $\boldsymbol{N} \in \mathbb{C}^{M \times N}$ models the additive noise component which we assume to be circularly symmetric complex Gaussian distributed and spatially uncorrelated. In general, the matrix $\boldsymbol{A} \in \mathbb{C}^{M \times d}$ is referred to as the mixing matrix. In the R-D case, $\boldsymbol{A}$ must obey the following decomposition

$$\boldsymbol{A} = \boldsymbol{A}^{(1)} \diamond \boldsymbol{A}^{(2)} \diamond \ldots \diamond \boldsymbol{A}^{(R)}, \tag{2}$$

where $\boldsymbol{A}^{(r)} \in \mathbb{C}^{M_r \times d}$. In the context of multidimensional harmonic retrieval, $\boldsymbol{A}^{(r)}$ represents the array steering matrix in the r-th mode.

In [3] we have shown that the measurement matrix $\boldsymbol{X}$ can be replaced by a measurement tensor $\boldsymbol{\mathcal{X}} \in \mathbb{C}^{M_1 \times M_2 \ldots \times M_R \times N}$. The data model (1), (2) is then transformed into

$$\boldsymbol{\mathcal{X}} = \boldsymbol{\mathcal{A}} \times_{R+1} \boldsymbol{S}^{\mathrm{T}} + \boldsymbol{\mathcal{N}}, \text{ where} \tag{3}$$

$$\boldsymbol{\mathcal{A}} = \boldsymbol{\mathcal{I}}_{R+1,d} \times_1 \boldsymbol{A}^{(1)} \ldots \times_R \boldsymbol{A}^{(R)} \in \mathbb{C}^{M_1 \times M_2 \ldots \times M_R \times d}. \tag{4}$$

Note that the tensor and matrix data models are related via $\boldsymbol{A} = [\boldsymbol{\mathcal{A}}]^{\mathrm{T}}_{(R+1)}$, $\boldsymbol{N} = [\boldsymbol{\mathcal{N}}]^{\mathrm{T}}_{(R+1)}$, and $\boldsymbol{X} = [\boldsymbol{\mathcal{X}}]^{\mathrm{T}}_{(R+1)}$.

To enhance the readability, we will focus on the $R = 2$ dimensional case for the rest of the paper. The extension of the presented results to more than two dimensions is rather straightforward.

In the matrix case, a basis for the signal subspace is estimated by computing the d dominant left singular vectors of the observed measurement matrix $\boldsymbol{X}$. We refer to this estimate via the matrix $\hat{\boldsymbol{U}}_{\mathrm{s}} \in \mathbb{C}^{M \times d}$. In the tensor case, an enhanced estimate of the signal subspace is found by computing the truncated HOSVD as

$$\boldsymbol{\mathcal{X}} \approx \hat{\boldsymbol{\mathcal{S}}}^{[\mathrm{s}]} \times_1 \hat{\boldsymbol{U}}_1^{[\mathrm{s}]} \times_2 \hat{\boldsymbol{U}}_2^{[\mathrm{s}]} \times_3 \hat{\boldsymbol{U}}_3^{[\mathrm{s}]}, \tag{5}$$

where $\hat{\boldsymbol{\mathcal{S}}}^{[\mathrm{s}]} \in \mathbb{C}^{p_1 \times p_2 \times d}$, $\hat{\boldsymbol{U}}_1^{[\mathrm{s}]} \in \mathbb{C}^{M_1 \times p_1}$, $\hat{\boldsymbol{U}}_2^{[\mathrm{s}]} \in \mathbb{C}^{M_2 \times p_2}$, and $\hat{\boldsymbol{U}}_3^{[\mathrm{s}]} \in \mathbb{C}^{N \times d}$. Here, $p_r = \min\{M_r, d\}$ and we use the assumption that $N \geq d$. Then, the signal subspace tensor $\boldsymbol{\mathcal{U}}^{[\mathrm{s}]}$ is defined via [3]

$$\hat{\boldsymbol{\mathcal{U}}}^{[\mathrm{s}]} = \hat{\boldsymbol{\mathcal{S}}}^{[\mathrm{s}]} \times_1 \hat{\boldsymbol{U}}_1^{[\mathrm{s}]} \times_2 \hat{\boldsymbol{U}}_2^{[\mathrm{s}]} \times_3 \hat{\boldsymbol{\Sigma}}_3^{[\mathrm{s}]^{-1}} \in \mathbb{C}^{M_1 \times M_2 \times d}. \tag{6}$$

Here, in extension to [3] we have added the 3-mode product with the inverse of the diagonal matrix of 3-mode singular values $\hat{\boldsymbol{\Sigma}}_3^{[\mathrm{s}]}$, which is defined as $\hat{\boldsymbol{\Sigma}}_3^{[\mathrm{s}]} = \left[\hat{\boldsymbol{\mathcal{S}}}^{[\mathrm{s}]}\right]_{(3)} \cdot \left[\hat{\boldsymbol{\mathcal{S}}}^{[\mathrm{s}]}\right]_{(3)}^{\mathrm{H}} \in \mathbb{C}^{d \times d}$. Note that this scaling does not affect the subspace. This normalization is performed only to simplify the notation later on.

As demonstrated numerically in [3, 8], in the presence of noise, the matrix $\left[\hat{\boldsymbol{\mathcal{U}}}^{[\mathrm{s}]}\right]_{(3)}^{\mathrm{T}} \in \mathbb{C}^{M \times d}$ provides a more accurate estimate of the signal subspace than the matrix $\hat{\boldsymbol{U}}_s$. Therefore, the estimated signal subspace can be replaced by the HOSVD-based subspace in any subspace-based parameter estimation scheme. This gives, for example, rise to the Tensor-ESPRIT-type algorithms described in [3]. It is the goal of this paper to quantify the improvement in the estimate of the signal subspace and the corresponding parameter estimation accuracy analytically.

4. PERTURBATION ANALYSIS FOR THE HOSVD-BASED SIGNAL SUBSPACE ESTIMATE

In this section we first review the perturbation analysis for the SVD introduced in [5] and then present the novel extension to the HOSVD. To this end, let $\boldsymbol{X}^{(0)}$ be the noise-free measurement matrix, so that $\boldsymbol{X} = \boldsymbol{X}^{(0)} + \boldsymbol{N}$. Then, the SVD of $\boldsymbol{X}^{(0)}$ is given by

$$\boldsymbol{X}^{(0)} = \begin{bmatrix} \boldsymbol{U}_{\mathrm{s}} & \boldsymbol{U}_{\mathrm{n}} \end{bmatrix} \cdot \begin{bmatrix} \boldsymbol{\Sigma}_{\mathrm{s}} & \boldsymbol{0} \\ \boldsymbol{0} & \boldsymbol{0} \end{bmatrix} \cdot \begin{bmatrix} \boldsymbol{V}_{\mathrm{s}}^{\mathrm{H}} \\ \boldsymbol{V}_{\mathrm{n}}^{\mathrm{H}} \end{bmatrix}, \tag{7}$$

where $\boldsymbol{U}_{\mathrm{n}} \in \mathbb{C}^{M \times M-d}$ is a basis for the noise subspace, $\boldsymbol{V}_{\mathrm{s}} \in \mathbb{C}^{N \times d}$ is a basis for the row space, and $\boldsymbol{\Sigma}_{\mathrm{s}} \in \mathbb{R}^{d \times d}$ is the diagonal matrix of ordered non-zero singular values. Similarly, in the tensor case we introduce the truncated HOSVD of the noise-free measurement tensor $\boldsymbol{\mathcal{X}}^{(0)}$

$$\boldsymbol{\mathcal{X}}^{(0)} = \boldsymbol{\mathcal{S}}^{[\mathrm{s}]} \times_1 \boldsymbol{U}_1^{[\mathrm{s}]} \times_2 \boldsymbol{U}_2^{[\mathrm{s}]} \times_3 \boldsymbol{U}_3^{[\mathrm{s}]}. \tag{8}$$

In [5] and [6] it is shown that a first order expansion of the estimate $\hat{\boldsymbol{U}}_{\mathrm{s}}$ of the true signal subspace $\boldsymbol{U}_{\mathrm{s}}$ via the SVD of the noisy measurements in (1) is given by

$$\hat{\boldsymbol{U}}_{\mathrm{s}} = \boldsymbol{U}_{\mathrm{s}} + \Delta \boldsymbol{U}_{\mathrm{s}}, \text{ where} \tag{9}$$

$$\Delta \boldsymbol{U}_{\mathrm{s}} \approx \boldsymbol{U}_{\mathrm{n}} \cdot \boldsymbol{P} + \boldsymbol{U}_{\mathrm{s}} \cdot \boldsymbol{Q}, \tag{10}$$

where $\boldsymbol{P} = \boldsymbol{U}_{\mathrm{n}}^{\mathrm{H}} \boldsymbol{N} \boldsymbol{V}_{\mathrm{s}} \boldsymbol{\Sigma}_{\mathrm{s}}^{-1}$ and $\boldsymbol{Q}$ is chosen to zero in [5] and to $\boldsymbol{D} \odot \left(\boldsymbol{U}_{\mathrm{s}}^{\mathrm{H}} \boldsymbol{N} \boldsymbol{V}_{\mathrm{s}} \boldsymbol{\Sigma}_{\mathrm{s}} + \boldsymbol{\Sigma}_{\mathrm{s}} \boldsymbol{V}_{\mathrm{s}}^{\mathrm{H}} \boldsymbol{N}^{\mathrm{H}} \boldsymbol{U}_{\mathrm{s}}\right)$ in [6]. Here, the (k, ℓ)-element of

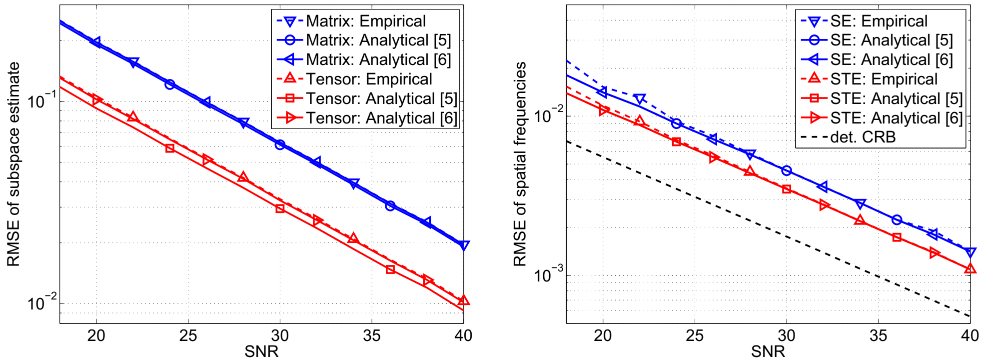

Fig. 1. Comparison of predicted and empirical RMSE for the subspace (left) and for the spatial frequencies (right). Scenario: 8×8 URA (2-D), $N = 5$ snapshots, $d = 4$ uncorrelated sources at $\mu_1 = -1.5$, $\mu_2 = 0.5$, $\mu_3 = 1.0$, $\mu_4 = -0.3$, $\nu_1 = 1.3$, $\nu_2 = -0.2$, $\nu_3 = 0.7$, and $\nu_4 = -1.5$

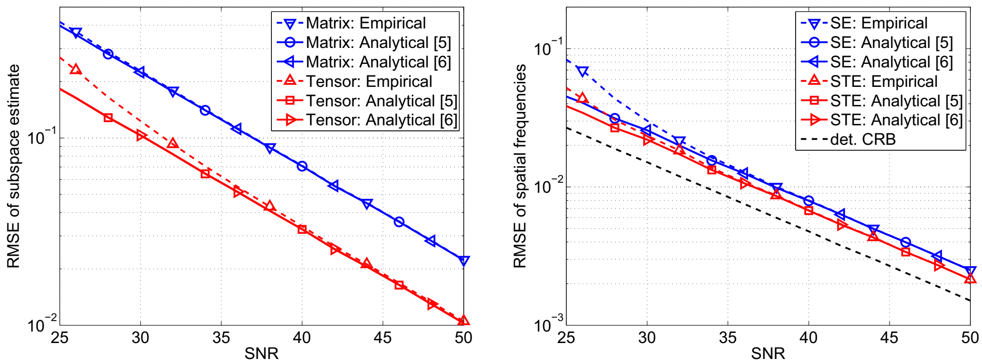

Fig. 2. Comparison of predicted and empirical RMSE for the subspace (left) and for the spatial frequencies (right). Scenario: 8×8 URA (2-D), $N = 20$ snapshots, $d = 3$ sources correlated with $\rho = 0.97$ at $\mu_1 = 0.7$, $\mu_2 = 0.9$, $\mu_3 = 1.1$, $\nu_1 = -0.1$, $\nu_2 = -0.3$, and $\nu_3 = -0.5$.

the matrix $\boldsymbol{D}$ is equal to $1/(\sigma_\ell^2 - \sigma_k^2)$ for $k \neq \ell$ and zero otherwise. Note that $\hat{\boldsymbol{U}}_{\rm s}$ can also be calculated directly from $\boldsymbol{X}$ via

$$\hat{\boldsymbol{U}}_{\rm s} = \boldsymbol{X} \cdot \hat{\boldsymbol{V}}_{\rm s} \cdot \hat{\boldsymbol{\Sigma}}_{\rm s}^{-1}. \tag{11}$$

To arrive at similar expressions for the HOSVD we first observe that the truncated core tensor can directly be computed from $\boldsymbol{\mathcal{X}}$ by multiplying with $\hat{\boldsymbol{U}}_i^{[{\rm s}]^{\rm H}}$ in mode i for $i = 1, 2, 3$

$$\hat{\boldsymbol{\mathcal{S}}}^{[{\rm s}]} = \boldsymbol{\mathcal{X}} \times_1 \hat{\boldsymbol{U}}_1^{[{\rm s}]^{\rm H}} \times_2 \hat{\boldsymbol{U}}_2^{[{\rm s}]^{\rm H}} \times_3 \hat{\boldsymbol{U}}_3^{[{\rm s}]^{\rm H}}. \tag{12}$$

It is easy to show that the $\hat{\boldsymbol{\mathcal{S}}}^{[{\rm s}]}$ obtained via (12) is exactly the same as the one obtained by computing the full HOSVD and then truncating the core tensor. Inserting (12) into (6) yields

$$\hat{\boldsymbol{\mathcal{U}}}^{[{\rm s}]} = \boldsymbol{\mathcal{X}} \times_1 \left(\hat{\boldsymbol{U}}_1^{[{\rm s}]} \cdot \hat{\boldsymbol{U}}_1^{[{\rm s}]^{\rm H}}\right) \times_2 \left(\hat{\boldsymbol{U}}_2^{[{\rm s}]} \cdot \hat{\boldsymbol{U}}_2^{[{\rm s}]^{\rm H}}\right) \times_3 \left(\hat{\boldsymbol{\Sigma}}_3^{[{\rm s}]^{-1}} \cdot \hat{\boldsymbol{U}}_3^{[{\rm s}]^{\rm H}}\right).$$

Consequently, $\left[\hat{\boldsymbol{\mathcal{U}}}^{[{\rm s}]}\right]_{(3)}^{\rm T}$ can be expressed as

$$\left[\hat{\boldsymbol{\mathcal{U}}}^{[{\rm s}]}\right]_{(3)}^{\rm T} = \left(\hat{\boldsymbol{T}}_1 \otimes \hat{\boldsymbol{T}}_2\right) \cdot [\boldsymbol{\mathcal{X}}]_{(3)}^{\rm T} \cdot \hat{\boldsymbol{U}}_3^{[{\rm s}]^*} \cdot \hat{\boldsymbol{\Sigma}}_3^{[{\rm s}]^{-1}}, \tag{13}$$

where we have introduced the short hand notation $\hat{\boldsymbol{T}}_i = \hat{\boldsymbol{U}}_i^{[{\rm s}]} \cdot \hat{\boldsymbol{U}}_i^{[{\rm s}]^{\rm H}}$ for the projection matrices onto the space spanned by the i-mode vectors for $i = 1, 2$. Comparing (11) with (13) we notice some similarities. First of all, as shown in Section 3, $[\boldsymbol{\mathcal{X}}]_{(3)}^{\rm T} = \boldsymbol{X}$. Moreover, since $\hat{\boldsymbol{U}}_3^{[{\rm s}]}$ and $\hat{\boldsymbol{\Sigma}}_3^{[{\rm s}]}$ are computed via the truncated SVD of $[\boldsymbol{\mathcal{X}}]_{(3)}$ [1], it is not difficult to see that $\hat{\boldsymbol{U}}_3^{[{\rm s}]^*} = \hat{\boldsymbol{V}}_{\rm s}$ and $\hat{\boldsymbol{\Sigma}}_3^{[{\rm s}]} = \hat{\boldsymbol{\Sigma}}_{\rm s}$. We therefore conclude that the matrix-based subspace estimate and the tensor-based subspace estimate are related via

$$\left[\hat{\boldsymbol{\mathcal{U}}}^{[{\rm s}]}\right]_{(3)}^{\rm T} = \left(\hat{\boldsymbol{T}}_1 \otimes \hat{\boldsymbol{T}}_2\right) \hat{\boldsymbol{U}}_{\rm s}. \tag{14}$$

Equation (14) provides an interesting insight: the improvement from the HOSVD-based subspace estimate stems from a projection onto the Kronecker product of the space spanned by the 1-mode vectors and the space spanned by the 2-mode vectors. This also shows that for $d \geq \max(M_1, M_2)$, the matrix and tensor subspaces are identical [3], since in this case $\boldsymbol{T}_1$ and $\boldsymbol{T}_2$ are identity matrices.

To arrive at a perturbation expansion for $\left[\hat{\boldsymbol{\mathcal{U}}}^{[{\rm s}]}\right]_{(3)}^{\rm T}$ we express the estimated projection matrices $\hat{\boldsymbol{T}}_i$ as

$$\begin{aligned} \hat{\boldsymbol{T}}_i &= \left(\boldsymbol{U}_i^{[{\rm s}]} + \Delta\boldsymbol{U}_i^{[{\rm s}]}\right) \cdot \left(\boldsymbol{U}_i^{[{\rm s}]^{\rm H}} + \Delta\boldsymbol{U}_i^{[{\rm s}]^{\rm H}}\right) \\ &= \boldsymbol{T}_i + \boldsymbol{U}_i^{[{\rm s}]} \cdot \Delta\boldsymbol{U}_i^{[{\rm s}]^{\rm H}} + \Delta\boldsymbol{U}_i^{[{\rm s}]} \cdot \boldsymbol{U}_i^{[{\rm s}]^{\rm H}} + \Delta\boldsymbol{U}_i^{[{\rm s}]} \cdot \Delta\boldsymbol{U}_i^{[{\rm s}]^{\rm H}}. \end{aligned} \tag{15}$$

Since we are interested in a first-order perturbation analysis, the last term can be neglected. Inserting this expansion into (14) we obtain the final result

$$\left[\hat{\boldsymbol{\mathcal{U}}}^{[\mathrm{s}]}\right]_{(3)}^{\mathrm{T}} = \boldsymbol{U}_{\mathrm{s}} + \left[\Delta\boldsymbol{\mathcal{U}}^{[\mathrm{s}]}\right]_{(3)}^{\mathrm{T}}, \text{ where} \tag{16}$$

$$\left[\Delta\boldsymbol{\mathcal{U}}^{[\mathrm{s}]}\right]_{(3)}^{\mathrm{T}} \approx (\boldsymbol{T}_1 \otimes \boldsymbol{T}_2)\Delta\boldsymbol{U}_{\mathrm{s}} + \left((\Delta\boldsymbol{U}_1^{[\mathrm{s}]} \cdot \boldsymbol{U}_1^{[\mathrm{s}]^{\mathrm{H}}}) \otimes \boldsymbol{T}_2\right) \cdot \boldsymbol{U}_{\mathrm{s}} + \left(\boldsymbol{T}_1 \otimes (\Delta\boldsymbol{U}_2^{[\mathrm{s}]} \cdot \boldsymbol{U}_2^{[\mathrm{s}]^{\mathrm{H}}})\right) \cdot \boldsymbol{U}_{\mathrm{s}}. \tag{17}$$

Since the $\hat{\boldsymbol{U}}_i^{[\mathrm{s}]}$ are computed via the SVD of i-mode unfoldings, the matrix perturbation analysis for them is valid and we can compute $\Delta\boldsymbol{U}_i^{[\mathrm{s}]}$ via (10). It can be shown that even if $\boldsymbol{Q}_i$ is taken into account according to [6] its impact on (17) cancels due to the fact that $\boldsymbol{Q}_i^{\mathrm{H}} = -\boldsymbol{Q}_i$. Consequently, $\Delta\boldsymbol{U}_i^{[\mathrm{s}]}$ is given by

$$\Delta\boldsymbol{U}_1^{[\mathrm{s}]} \approx \boldsymbol{U}_1^{[\mathrm{n}]} \cdot \left(\boldsymbol{U}_1^{[\mathrm{n}]}\right)^{\mathrm{H}} \cdot [\boldsymbol{\mathcal{N}}]_{(1)} \cdot \boldsymbol{V}_1^{[\mathrm{s}]} \cdot \left(\boldsymbol{\Sigma}_1^{[\mathrm{s}]}\right)^{-1} \tag{18}$$

$$\Delta\boldsymbol{U}_2^{[\mathrm{s}]} \approx \boldsymbol{U}_2^{[\mathrm{n}]} \cdot \left(\boldsymbol{U}_2^{[\mathrm{n}]}\right)^{\mathrm{H}} \cdot [\boldsymbol{\mathcal{N}}]_{(2)} \cdot \boldsymbol{V}_2^{[\mathrm{s}]} \cdot \left(\boldsymbol{\Sigma}_2^{[\mathrm{s}]}\right)^{-1}, \tag{19}$$

where the quantities $\boldsymbol{U}_i^{[\mathrm{n}]}$, $\boldsymbol{V}_i^{[\mathrm{s}]}$, and $\boldsymbol{\Sigma}_i^{[\mathrm{s}]}$ correspond to $\boldsymbol{U}_{\mathrm{n}}$, $\boldsymbol{V}_{\mathrm{s}}$, and $\boldsymbol{\Sigma}_{\mathrm{s}}$ in (7) if $\boldsymbol{X}^{(0)}$ is replaced by $\left[\boldsymbol{\mathcal{X}}^{(0)}\right]_{(i)}$ for $i = 1, 2$. Note that since the left subspaces $\boldsymbol{V}_i^{[\mathrm{s}]}$ do usually not appear in the HOSVD they may be replaced by the following expressions

$$\boldsymbol{V}_1^{[\mathrm{s}]} = \left(\boldsymbol{U}_2^{[\mathrm{s}]} \otimes \boldsymbol{U}_3^{[\mathrm{s}]}\right)^* \cdot [\boldsymbol{\mathcal{S}}]_{(1)}^{[\mathrm{s}]^{\mathrm{H}}} \cdot \left(\boldsymbol{\Sigma}_1^{[\mathrm{s}]}\right)^{-1}$$

$$\boldsymbol{V}_2^{[\mathrm{s}]} = \left(\boldsymbol{U}_3^{[\mathrm{s}]} \otimes \boldsymbol{U}_1^{[\mathrm{s}]}\right)^* \cdot [\boldsymbol{\mathcal{S}}]_{(2)}^{[\mathrm{s}]^{\mathrm{H}}} \cdot \left(\boldsymbol{\Sigma}_2^{[\mathrm{s}]}\right)^{-1}.$$

5. SIMULATION RESULTS

In this section we demonstrate the validity of the analytical performance framework by comparing the predicted estimation errors with empirical ones obtained via Monte Carlo simulations. As shown in [5] the perturbation analysis for the matrix subspace can directly be used to characterize the performance of standard ESPRIT analytically. Replacing the perturbation analysis for the matrix signal subspace by the perturbation analysis for the tensor signal subspace, this yields a performance assessment for the 2-D standard Tensor-ESPRIT algorithm [3].

We therefore simulate d planar wavefronts impinging on a uniform rectangular array (URA) of 8×8 isotropic antenna elements. The elements of the symbol matrix $\boldsymbol{S}$ as well as the noise matrix $\boldsymbol{N}$ are both drawn from a zero mean circularly symmetric complex Gaussian distribution with variance 1 for the elements of $\boldsymbol{S}$ and variance σ_n^2 for the elements of $\boldsymbol{N}$. Consequently, the SNR is defined as $1/\sigma_n^2$. The goal is to estimate the 2-D spatial frequencies μ_i and ν_i for $i = 1, 2, \ldots, d$.

For the simulation result displayed in Figure 1 we choose $d = 4$ uncorrelated sources positioned at $\mu_1 = -1.5$, $\mu_2 = 0.5$, $\mu_3 = 1.0$, $\mu_4 = -0.3$, $\nu_1 = 1.3$, $\nu_2 = -0.2$, $\nu_3 = 0.7$, and $\nu_4 = -1.5$ and set the number of snapshots N to 5. On the other hand, Figure 2 displays a scenario where $d = 3$ correlated sources are located at $\mu_1 = 0.7$, $\mu_2 = 0.9$, $\mu_3 = 1.1$, $\nu_1 = -0.1$, $\nu_2 = -0.3$, and $\nu_3 = -0.5$. Here, the correlation coefficient ρ is set to 0.97 and $N = 20$ snapshots are considered. In both cases, on the left-hand side we compare the analytical expressions from (10) and (17) with the empirical results by calculating the RMSE of the subspace defined as $\|\Delta\boldsymbol{U}_{\mathrm{s}}\|_{\mathrm{F}}$ for the matrix case and $\left\|[\Delta\boldsymbol{\mathcal{U}}^{[\mathrm{s}]}]_{(3)}\right\|_{\mathrm{F}}$ for the tensor case. Note that the empirical subspace estimation error is computed per column according to

$$\Delta\boldsymbol{u}_n = \hat{\boldsymbol{u}}_n \cdot \frac{\hat{\boldsymbol{u}}_n^{\mathrm{H}}\boldsymbol{u}_n}{|\hat{\boldsymbol{u}}_n^{\mathrm{H}}\boldsymbol{u}_n|} - \boldsymbol{u}_n, \quad n = 1, 2, \ldots, d \tag{20}$$

as in [6]. The right-hand side depicts the estimation error for the spatial frequencies defined according to

$$\mathrm{RMSE} = \sqrt{\mathbb{E}\left\{\sum_{i=1}^{d} (\mu_i - \hat{\mu}_i)^2 + (\nu_i - \hat{\nu}_i)^2\right\}}. \tag{21}$$

For comparison, we also display the deterministic Cramér-Rao Bound (CRB) [9]. In all cases we observe a good fit between analytical and empirical results, especially for higher SNRs. This is expected since the first order approximation always assumes the perturbation terms to be small, which implicitly assumes a high SNR. Moreover, we observe that for the first scenario, the subspace prediction [6] outperforms [5], however, this has no impact on the analytical estimation accuracy for ESPRIT. In general, a difference between [6] and [5] is visible only in terms of the subspace estimation error for scenarios with far-spaced, uncorrelated sources if N is large and M is small.

6. CONCLUSIONS

In this paper we present an analytical performance assessment for the HOSVD-based subspace estimate which is the basis for Tensor-ESPRIT-type algorithms. The closed-form expression for the subspace estimation error is derived by extending the first-order matrix-based performance predictions to the tensor case. We also show via simulations that the analytical performance evaluation for the tensor-subspace allows to reliably predict the performance of standard Tensor-ESPRIT. Note that since the expressions explicitly depend on the realization of the noise and the source symbols, no assumption about the statistics of the noise samples or the source symbols are required.

REFERENCES

[1] L. de Lathauwer, B. de Moor, and J. Vanderwalle, “A multilinear singular value decomposition”, *SIAM J. Matrix Anal. Appl.*, vol. 21, no. 4, 2000.

[2] B. Friedlander and A. Weiss, “On the second-order statistics of the eigenvectors of sample covariance matrices”, *IEEE Transactions on Signal Processing*, vol. 46, no. 11, pp. 3136–3139, Nov. 1998.

[3] M. Haardt, F. Roemer, and G. Del Galdo, “Higher-order SVD based subspace estimation to improve the parameter estimation accuracy in multi-dimensional harmonic retrieval problems”, *IEEE Transactions on Signal Processing*, vol. 56, pp. 3198–3213, July 2008.

[4] M. Haardt, R. S. Thomä, and A. Richter, “Multidimensional high-resolution parameter estimation with applications to channel sounding”, in *High-Resolution and Robust Signal Processing*, Y. Hua, A. Gershman, and Q. Chen, Eds., pp. 255–338. Marcel Dekker, New York, NY, 2004, Chapter 5.

[5] F. Li, H. Liu, and R. J. Vaccaro, “Performance analysis for DOA estimation algorithms: Unification, simplifications, and observations”, *IEEE Transactions on Aerospace and Electronic Systems*, vol. 29, no. 4, pp. 1170–1184, Oct. 1993.

[6] J. Liu, X. Liu, and X. Ma, “First-order perturbation analysis of singular vectors in singular value decomposition”, *IEEE Transactions on Signal Processing*, vol. 56, no. 7, pp. 3044–3049, July 2008.

[7] X. Liu, N. D. Sidiropoulos, and A. Swami, “Blind high-resolution localization and tracking of multiple frequency hopped signals”, *IEEE Transactions on Signal Processing*, vol. 50, no. 4, pp. 889–901, Apr. 2002.

[8] F. Roemer, M. Haardt, and G. Del Galdo, “Higher order SVD based subspace estimation to improve multi-dimensional parameter estimation algorithms”, in *Proc. 40th Asilomar Conf. on Signals, Systems, and Computers*, pp. 961–965, Pacific Grove, CA, Nov. 2006.

[9] P. Stoica and A. Nehorai, “MUSIC, maximum likelihood, and Cramér-Rao bound”, *IEEE Transactions on Acoustics, Speech, and Signal Processing*, vol. 37, pp. 720–741, May 1989.

[10] R. J. Vaccaro, “A second-order perturbation expansion for the SVD”, *SIAM J. Matrix Anal. Appl.*, vol. 15, no. 2, pp. 661–671, Apr. 1994.

[11] Z. Xu, “Perturbation analysis for subspace decomposition with applications in subspace-based algorithms”, *IEEE Transactions on Signal Processing*, vol. 50, no. 11, pp. 2820–2830, Nov. 2002.